Proceedings of the 1993 International
Symposium on Intelligent Control
Chicago, Illinois, USA - August 1993

Robust Guidance of a Conventionally Steered Vehicle using Destination Bearing

R. Neil Braithwaite and Bir Bhanu
College of Engineering
University of California at Riverside
Riverside, CA 92521

Abstract

This paper presents an algorithm for camera-based navigation of a conventionally steered vehicle. The destination bearing, obtained by actively panning the camera to fixate on the destination, is the primary measurement. A steering sequence designed to direct a moving vehicle towards a visible destination is generated using an extension of predictive control techniques. A variable sampling interval, based on distance traveled instead of elapsed time, provides robustness to destination range errors. Additional robustness is achieved by incorporating non-linearities into the steering algorithm, ensuring that the moving vehicle originating from an awkward position and heading will not diverge from the destination. A two-stage extended Kalman filter, which uses the destination bearing angle and known vehicle motion, provides estimates of range. A criterion for shifting the attention of the camera between intermediate destinations is presented. Simulation results demonstrate the effectiveness of the proposed steering algorithm.

1. Introduction

Local navigation of a conventionally steered vehicle consists of generating a sequence of steering commands to direct a moving vehicle to a goal destination. An important aspect of local navigation is the use of sensory information to continually update the ego-state of the vehicle with respect to the environment and the destination. In this paper, it is assumed that the primary sensor is a camera mounted on a pan-tilt platform; auxiliary sensors include encoders measuring the pan and steering angles, and an odometer measuring distance traveled. It is further assumed that a sequence of goal destinations, similar to the "postures" in [6], is generated by an external global planner.

An image sequence produced by a moving camera provides an enormous amount of data. As a result, the image processing will likely be the most computational intensive stage in an autonomous vehicle. Active vision can reduce the complexity of vision-based tasks, such as navigation, by exploiting the fact that the amount of contextually relevant information encoded in the image sequence is significantly less than the data presented. Active vision controls sensor parameters, such as the pan-tilt of a camera, to selectively extract task-related information from the environment. The most impressive implementation of this context-sensitive processing in the autonomous navigation field is Dickmanns' road-following work [3].

This paper investigates the problem of generating a sequence of steering commands that will maneuver the vehicle to, or around, a "marker" visible in a camera image. A marker is a distinctive environmental feature: natural or man-made. It can be a destination landmark, a beacon denoting a hazard, or a detectable obstacle. By fixating the camera on a marker, the camera pan angle provides an estimate of the bearing of the marker relative to the vehicle position and heading. Using bearing measurements and known vehicle motion, it is possible to generate steering commands that will direct the vehicle towards a marker of interest. This formulation produces two significant benefits: (a) the image processing is reduced because only a small fraction of the image is considered; (b) by specifying the destination marker instead of a complete path, the task of local navigation is reduced to a guidance problem. The image processing/pan control required to fixate the camera gaze onto a marker is not covered in this paper. The guidance of the vehicle using the resulting bearing measurement is discussed.

The outline of this paper is as follows. Section 2 discusses the maneuvering of a conventionally steered vehicle. Section 3 describes the basic steering algorithm which is an interesting variation of state space predictive control. Section 4 presents novel nonlinear modifications to the basic algorithm to ensure robustness to range errors and awkward initial conditions. Section 5 describes a Kalman filter for sequentially estimating range and bearing to each marker from noisy bearing measurements. A novel criteria for switching attention between multiple markers is presented. Sections 6 and 7 contain simulation results and concluding remarks, respectively.

2. Maneuvering a Vehicle

The maneuvering of a vehicle from its current location to a specified destination is performed by generating a sequence of steering and propulsion commands. In this paper, it is assumed that the vehicle is a three-wheel electric cart which is steered by adjusting the angle of the front wheel. Modifications to the basic cart include the addition of a DC steering motor.

A maneuver can be described as a coordinated sequence of heading changes. A heading change, viewed as a function of time, is dependent on both the steering angle and the speed of the vehicle. Under certain conditions—if the vehicle guide point is properly selected [7] and the effects of vehicle-ground interactions are negligible (speed is small) [8]—the heading change is separable with respect to the steering angle and vehicle speed. In such a case, maneuvers can be specified as functions of distance traveled, reducing the maneuvering problem to generating a sequence of steering angles that satisfies a set of initial and final conditions including position, and heading, subject to limits on the steering angle and the steering angle rate.

The steering sequence can be described in terms of path curvature instead of steering angle. The heading of the vehicle is given by

$$\phi_{h(L)} = \int_0^L \kappa_l \, dl + \phi_h, \tag{1}$$

where κ_l is the future path curvature after the vehicle has traveled a distance l, ϕ_h is the current heading vehicle, and $\phi_{h(l)}$ is the future heading. The Cartesian coordinates of the vehicle as a function of distance traveled are given by

$$\begin{bmatrix} x_L \\ z_L \end{bmatrix} = \begin{bmatrix} \int_0^L \sin \phi_{h(l)} \, dl + x_0 \\ \int_0^L \cos \phi_{h(l)} \, dl + z_0 \end{bmatrix}, \tag{2}$$

where (x_0, z_0) is the current position of the vehicle and (x_l, z_l) is

0-7803-1206-6/93/$3.00 ©1993 IEEE

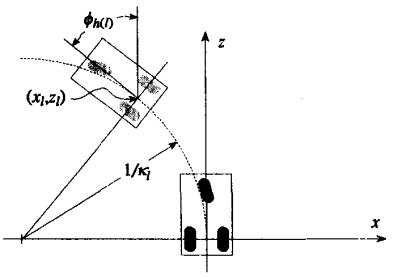

Figure 1: Viewer-centered reference frame. $(x_0, z_0) = (0, 0)$, and $\phi_h = 0$.

the future position. The coordinate system used in this paper is shown in figure 1. It is a viewer-centered reference frame where the current position is the origin and the z-axis is parallel to the current heading ($(x_0, z_0) = (0, 0)$, $\phi_h = 0$). The nonlinearity introduced by the sine/cosine makes the conversion of position constraints associated with markers into constraints on the steering commands difficult.

In many implementations, the planned path is specified as a continuous function of x_l and z_l. The motivation for such a specification is that obstacles and destinations are often described in terms of Cartesian coordinates obtained from a map (such as in [4]). However, effort is often required to ensure that the planned path is feasible for a conventionally steered vehicle; that is, the chosen path should be continuous with respect to position and heading, and have limited curvature. Such paths can be formed using high-order splines [7] or a sequence of smooth elementary curves [6]. An alternative approach is to specify the planned path in terms of a sequence of curvatures [5]. The difficulty associated with this approach is that any linearized conversion of marker constraints into curvature and path length will only be approximate. This is not serious when the position of a marker is measured relative to the vehicle using sensors. Sensor uncertainty makes any position constraint approximate regardless of the path representation.

There are advantages to specifying the path in terms of curvature and path length: it is easy to produce a feasible path for a conventionally steered vehicle; and the path curvature and length can be measured from the steering angle and wheel rotation, respectively. In many cases, the environmental constraints on the vehicle motion are sparse, occurring at specific points rather than continuously along the path. Thus, it is only necessary to constrain the vehicle's position and heading at these "markers." Between markers, the limits on steering angle and steering rate are the important constraints; violation of steering constraints are made explicit in the curvature-path length representation.

Constraints associated with markers are represented using state variables. The state variables include the lateral error and the heading error of the vehicle relative to each marker m:

$$\bar{\mathbf{e}}_{0,m} = [(r_m \sin \phi_{b,m}) \;\; (\phi_{h,m} - \phi_h)]^T, \tag{3}$$

where $\bar{\mathbf{e}}_{0,m}$ is the error state vector of the vehicle at its current position and heading relative to marker m; $\phi_{b,m}$ is the bearing angle of marker m relative to the current vehicle heading ϕ_h, r_m is the range to marker m, and $\phi_{h,m}$ is the desired heading at marker m. The predicted error state vector for the vehicle at a future path position l is denoted by $\bar{\mathbf{e}}_{l,m}$.

The future position and orientation of the vehicle relative to some specified reference, usually its current position and heading, are denoted by

$$\bar{\mathbf{d}}_l = [n_l \;\; \phi_{h(l)}]^T. \tag{4}$$

3. State Space Prediction

Predictive control techniques can be used to produce useful steering sequences. The objective of a predictive controller is to "drive" the error state variables close to zero at a future instant subject to limits on the control variable. For the case of a conventionally steered vehicle, the future instant and the control variable correspond to the path length index l and the path curvature κ, respectively.

Prediction is limited by "horizons" which are measured in terms of distance or number of "steps", where a step is a distance interval Δl. Predictive control is characterized by two horizons: an "output horizon" and a "control horizon" [2]. The output horizon, which we will refer to as the "marker horizon", is the number of steps (or path distance) to an active marker. The control horizon is the number of steps (or path distance) allocated to the controller to minimize the error state variables. Beyond the control horizon, the control signal (path curvature) is set to zero.

The error state variables associated with a marker change as the vehicle moves. The linearized state transition is given by

$$\bar{\mathbf{d}}_{i+1} = \mathbf{A}\bar{\mathbf{d}}_i + \bar{\mathbf{b}}\kappa_i, \tag{5}$$

where $\bar{\mathbf{e}}_{i+1,m} = \bar{\mathbf{e}}_{0,m} - (\bar{\mathbf{d}}_{i+1} - \bar{\mathbf{d}}_0)$,

$$\mathbf{A} = \begin{bmatrix} 1 & \Delta l \\ 0 & 1 \end{bmatrix}, \; \bar{\mathbf{b}} = [\frac{(\Delta l)^2}{2} \;\; (\Delta l)]^T, \tag{6}$$

and Δl is the path distance between l_{i+1} and l_i. Equation (5) is a valid approximation when the heading error, $\phi_{h,m} - \phi_h$, is small.

Consider the case of one active marker (m) where the control and marker horizons are equal to $N\Delta l$. The cost function to be minimized by the control sequence of length N is given by

$$J = \bar{\mathbf{e}}_{N,m}^T \mathbf{W}_{e,m} \bar{\mathbf{e}}_{N,m} + \bar{\mathbf{u}}^T \mathbf{W}_u \bar{\mathbf{u}}, \tag{7}$$

where $\bar{\mathbf{u}} = [\kappa_1 \; \cdots \; \kappa_N]^T$; $\mathbf{W}_{e,m}$ and $\mathbf{W}_u$ are weighting matrices penalizing state errors and the control, respectively; and

$$\bar{\mathbf{e}}_{N,m} = \bar{\mathbf{e}}_{0,m} - \sum_{i=0}^{N-1} \mathbf{A}^i \bar{\mathbf{b}} \, \kappa_{N-i}. \tag{8}$$

The control sequence minimizing (7) is given by

$$\bar{\mathbf{u}} = [\mathbf{C}^T \mathbf{W}_{e,m} \mathbf{C} + \mathbf{W}_u]^{-1} \mathbf{C}^T \mathbf{W}_{e,m} \bar{\mathbf{e}}_{0,m}, \tag{9}$$

where $\mathbf{C} = [\mathbf{A}^{N-1}\bar{\mathbf{b}} \; \cdots \; \mathbf{A}\bar{\mathbf{b}} \; \bar{\mathbf{b}}]$.

Equation (9) provides the curvature for each step in the control horizon. In most cases, the steering sequence is recomputed after each step, therefore only the first curvature, κ_1, is required. The repeated calculation of κ_1 as the vehicle moves will be referred to as the "sensory feedback" mode; the execution of the entire steering sequence $\bar{\mathbf{u}}$, without sensory updates, will be referred to as the "feedforward" mode. The drawback of (9) is that endpoint constraints on the curvature are not enforced. An extension enforcing endpoint constraints is discussed later in this section.

The prediction can be generalized to include intermediate markers on the path, and markers that are beyond the control horizon. For the case of an intermediate marker m with a horizon of $n < N$, the 2 by N matrix $\mathbf{C}_m$ is

$$\mathbf{C}_m = [\mathbf{A}^{n-1}\bar{\mathbf{b}} \; \cdots \; \mathbf{A}\bar{\mathbf{b}} \; \bar{\mathbf{b}} \; 0 \cdots 0]. \tag{10}$$

Since the curvature beyond the control horizon N is set to zero, $\mathbf{C}_m$ for a marker m with a horizon of $n > N$ is given by

$$\mathbf{C}_m = [\mathbf{A}^{j+N-1}\bar{\mathbf{b}} \; \cdots \; \mathbf{A}^j\bar{\mathbf{b}}], \tag{11}$$

where $n = j + N$. For more than one active marker, the cost function becomes

$$J = \sum_m (\bar{\mathbf{e}}_{n,m}^T \mathbf{W}_{e,m} \bar{\mathbf{e}}_{n,m}) + \bar{\mathbf{u}}^T \mathbf{W}_u \bar{\mathbf{u}}, \tag{12}$$

where n is the horizon of marker m.

The control weighting matrix is written as

$$\mathbf{W}_u = \mathbf{W}_\kappa + \mathbf{W}_{\Delta\kappa}, \tag{13}$$

where $\mathbf{W}_\kappa = diag\{\lambda_{\kappa(1)}, \cdots, \lambda_{\kappa(N)}\}$,

$$\mathbf{W}_{\Delta\kappa} = \lambda_{\Delta\kappa} \begin{bmatrix} 2 & -1 & 0 & \cdots & 0 & 0 \\ -1 & 2 & -1 & \cdots & 0 & 0 \\ 0 & -1 & 2 & \cdots & 0 & 0 \\ \vdots & \vdots & \vdots & & \vdots & \vdots \\ 0 & 0 & 0 & \cdots & -1 & 2 \end{bmatrix} \tag{14}$$

$\mathbf{W}_\kappa$ and $\mathbf{W}_{\Delta\kappa}$ penalize large path curvatures and large changes in path curvature, respectively; $\lambda_{\kappa(i)}$ and $\lambda_{\Delta\kappa}$ are the respective weights. To properly restrict changes in curvature, it is necessary to enforce endpoint constraints: that is, the change in curvature from the current curvature, κ_0, and the first entry in the control sequence, κ_1, must be penalized. Similarly, the last entry in the control sequence, κ_N, should be small because it is at the edge of the control horizon (beyond which all curvatures are zero). The control sequence that accounts for these endpoint curvatures is given by

$$\bar{\mathbf{u}} = \mathbf{Q}_u^{-1} [\mathbf{W}_{ref} \bar{\mathbf{u}}_{ref} + \sum_m (\mathbf{C}_m^T \mathbf{W}_{e,m} \bar{\mathbf{e}}_{0,m})], \tag{15}$$

where $\mathbf{W}_{ref} = diag\{\lambda_{ref(1)}, 0, \cdots, 0, \lambda_{ref(1)}\}$,

$$\mathbf{Q}_u = [\sum_m (\mathbf{C}_m^T \mathbf{W}_{e,m} \mathbf{C}_m) + \mathbf{W}_u + \mathbf{W}_{ref}], \tag{16}$$

and $\bar{\mathbf{u}}_{ref} = [\kappa_0 \ 0 \ \cdots \ 0]^T$. Note that $\mathbf{W}_{ref}$ and $\bar{\mathbf{u}}_{ref}$ can be adjusted to constrain any entry in $\bar{\mathbf{u}}$, not just the entries near the endpoints.

The weighting matrix for the error state variables is given by $\mathbf{W}_{e,m} = diag\{\lambda_b, \lambda_h\}$, where λ_b and λ_h are the weights for the lateral error and the heading error, respectively. The weights are generally fixed. However, when the control horizon is significantly shorter than the path length to the marker of interest, the heading error weight, λ_h, is reduced.

4. Robustness

This section discusses modifications necessary to ensure robustness to range uncertainty and awkward initial conditions. Robustness to range uncertainty is obtained using a variable sampling interval, Δl, that is a fraction of the range to the current marker. Robustness to awkward initial conditions is obtained by incorporating nonlinearities into the steering algorithm and by bounding the influence of the heading error. Initial conditions with bearing angle or heading error whose absolute value is greater than $\frac{\pi}{2}$ are considered "awkward," otherwise they are considered "well-behaved."

When a camera is used as the primary sensor, the uncertainty in the estimated range can be large. The effects of range uncertainty on the steering sequence $\bar{\mathbf{u}}$ are reduced when the step size is a fraction of the estimated range: that is,

$$\Delta l = \frac{r_m}{N}, \tag{17}$$

where N is the order of the control horizon. Noting that

$$\begin{bmatrix} r_m \sin\phi_{b,m} \\ \phi_{h,m} - \phi_h \end{bmatrix} = \begin{bmatrix} (N - \frac{1}{2})\Delta l & \cdots & \frac{1}{2}\Delta l \\ 1 & \cdots & 1 \end{bmatrix} \bar{\mathbf{u}} \Delta l, \tag{18}$$

it can be seen that the substitution of (17) into (18) makes the product $\bar{\mathbf{u}}\Delta l$ invariant to range errors. As a result, a range error alters $\bar{\mathbf{u}}$ by a scale factor; however, the sign of each element in $\bar{\mathbf{u}}$ is correct. If the algorithm is using sensory feedback (recalculating κ_1 after each step) and the initial conditions are well-behaved, the vehicle will reach the marker m despite range errors.

When the initial conditions are not well-behaved, the linearization used in (5) becomes an inadequate approximation. Problems occur because (a) the lateral error is not a sufficient position constraint for all paths, (b) the control horizon does not reach the current marker, and (c) the influence of the heading error can be unbounded.

The lateral error does not distinguish between a vehicle moving towards or away from the marker. As the absolute value of the bearing angle increases beyond $\frac{\pi}{2}$, the lateral error will decrease, even though the vehicle is traveling away from the destination. The problem can be remedied by adding a constraint that realigns the vehicle towards the destination when the bearing angle is large. One possible constraint is to set the steering angle to maximum (the vehicle's largest feasible path curvature) when $|\phi_b| > \frac{\pi}{2}$.

When the initial conditions are not well-behaved, the path traveled by the vehicle will contain large curves, making the path distance to the marker significantly longer than the control horizon $N\ \Delta l$. In such cases, the control horizon that is too short for the algorithm to generate a feedforward sequence that can fulfill both the lateral error and heading error constraints simultaneously. The heading error weight must be temporarily reduced to ensure that the lateral error constraint is properly enforced, thereby keeping the vehicle traveling towards the destination.

Large heading errors cause linearized approximations to fail. The error state transition (5) assumes that the difference between the current heading and each predicted heading in the feedforward sequence is small enough that $\sin(\Delta l \ \sum_i \kappa_i) \approx \Delta l \ \sum_i \kappa_i$. At the step i where $|\Delta l \sum_i \kappa_i|$ exceeds $\frac{\pi}{2}$, an unwanted sign reversal occurs. Beyond step i, the lateral error increases and the vehicle diverges from the destination. If the influence of the heading error is reduced, the vehicle will not steer as severely. Therefore, $|\Delta l \sum_i \kappa_i|$ is reduced, and the sign reversal is eliminated, or at least delayed. As long as $|\phi_b| < \frac{\pi}{2}$, reducing the influence of the heading error to zero will cause the vehicle to align itself towards the destination. A less severe approach is to define a dynamic heading error weight, such as

$$\lambda_h = \begin{cases} \lambda_h & \text{if } |\phi_{h,m} - \phi_h| < \phi_T \\ \lambda_h \phi_T (\phi_{h,m} - \phi_h)^{-1} & \text{otherwise,} \end{cases} \tag{19}$$

where ϕ_T is a threshold between $\frac{\pi}{2}$ and π. Equation (19) ensures that the influence of the heading error is bounded.

5. Range and Bearing Estimation

When measurements are made using a single camera, range information is not directly measured. Instead, it must be estimated from changes in the bearing angle as the vehicle undergoes known motion. A common approach to estimating the position of a marker is to use a Kalman filter [1] with Cartesian state variables. For bearing-only measurements, the Kalman state variables and error covariance become

$$\begin{bmatrix} z \\ x \end{bmatrix} = \frac{1}{\rho} \begin{bmatrix} \cos\phi_b \\ \sin\phi_b \end{bmatrix}, \tag{20}$$

and

$$\begin{bmatrix} E[(\delta z)^2] & E[\delta z \, \delta x] \\ E[\delta x \, \delta z] & E[(\delta x)^2] \end{bmatrix} = \frac{1}{\rho^2} \mathbf{Q}^{-1}, \tag{21}$$

respectively, where $E[\ ]$ denotes expectation, ρ is the inverse of range, and

$$\mathbf{R}(\phi_b) = \begin{bmatrix} \cos\phi_b & \sin\phi_b \\ -\sin\phi_b & \cos\phi_b \end{bmatrix}, \quad (22)$$

$$\mathbf{Q}^{-1} = \mathbf{R}^T(\phi_b) \begin{bmatrix} E[(\frac{\delta\rho}{\rho})^2] & E[-\frac{\delta\rho}{\rho}\delta\phi_b] \\ E[-\delta\phi_b\frac{\delta\rho}{\rho}] & E[(\delta\phi_b)^2] \end{bmatrix} \mathbf{R}(\varphi_b). \quad (23)$$

Note that $\mathbf{Q}^{-1}$ is the angular error covariance.

The Kalman filter consists of two sets of recursive equations: state transition equations predict changes in ρ and ϕ_b and the error covariance in response to control inputs κ and Δl; and measurement equations integrate new bearing measurements, denoted by $\hat{\phi}_b$, into the state estimate. The state transition equation is given by

$$\begin{bmatrix} \cos\phi_b \\ \sin\phi_b \\ \rho \end{bmatrix}_{i+1/i} = m\,\mathbf{G} \begin{bmatrix} \cos\phi_b \\ \sin\phi_b \\ \rho \end{bmatrix}_i \quad (24)$$

where m is a normalization term ensuring that $(\cos\phi_b)^2+(\sin\phi_b)^2$ is unity at $i+1/i$, and

$$\mathbf{G} = \begin{bmatrix} \cos(\kappa\,\Delta l) & \sin(\kappa\,\Delta l) & -\Delta l\cos(0.5\,\kappa\,\Delta l) \\ -\sin(\kappa\,\Delta l) & \cos(\kappa\,\Delta l) & \Delta l\sin(0.5\,\kappa\,\Delta l) \\ 0 & 0 & 1 \end{bmatrix}. \quad (25)$$

The subscript $i+1/i$ indicates a prediction at path step $i+1$ based on measurements obtained at and before step i. The prediction of the error covariance is given by

$$\mathbf{Q}^{-1}_{i+1/i} = m^{-2}\mathbf{R}^T(\kappa\,\Delta l)\mathbf{Q}^{-1}_i\mathbf{R}(\kappa\,\Delta l) + \mathbf{N}_i, \quad (26)$$

where $\mathbf{N}_i$ is the process noise. If we consider only the uncertainty in ρ, the most significant noise source, then

$$\mathbf{N}_i = \mathbf{R}^T(\frac{\kappa\,\Delta l}{2}) \begin{bmatrix} (\Delta l)^2 q^{-1}_{\rho(i)} & 0 \\ 0 & 0 \end{bmatrix} \mathbf{R}(\frac{\kappa\,\Delta l}{2}), \quad (27)$$

where q_ρ^{-1} is the error covariance in ρ, which is defined later. The measurement update equations for the covariance and the state variables are given by:

$$\mathbf{Q}_{i+1} = \mathbf{Q}_{i+1/i} + \bar{\mathbf{h}}^T\bar{\mathbf{h}}(\delta\hat{\phi}_b)^{-2}, \quad (28)$$

where

$$\bar{\mathbf{h}} = [\sin(\hat{\phi}_b) \;\; -\cos(\hat{\phi}_b)]; \quad (29)$$

and

$$\begin{bmatrix} \cos\phi_b \\ \sin\phi_b \\ \rho \end{bmatrix}_{i+1} = m_2 \left\{ \begin{bmatrix} \cos\phi_b \\ \sin\phi_b \\ \rho \end{bmatrix}_{i+1/i} + \begin{bmatrix} \bar{\mathbf{k}}_g \\ 0 \end{bmatrix} \right\}, \quad (30)$$

where m_2 is a normalization term and

$$\bar{\mathbf{k}}_g = \mathbf{Q}^{-1}_{i+1}\bar{\mathbf{h}}^T\sin(\phi_{b(i+1/i)} - \hat{\phi}_b)(\delta\hat{\phi}_b)^{-2}. \quad (31)$$

The above filter has similarities to the modified gain extended Kalman filter described in [9]. Like other extended Kalman filters, the above filter is dependent on the initial estimate of ρ. To remove this dependency, a second Kalman filter estimates ρ. Before integrating the current bearing measurement, the change between the past estimate of $\phi_{b(i)}$ and $\hat{\phi}_b$ is used to estimate ρ:

$$\tilde{\rho}_i = (q_{\rho(i-1)} + q_{\phi(i)})^{-1}(q_{\rho(i-1)}\,\rho + q_{\phi(i)}\,\hat{\rho}) \quad (32)$$

$$q_{\phi(i)} = \frac{\sin^2(\hat{\phi}_b + 0.5\,\kappa\,\Delta l)}{(\delta\hat{\phi}_b)^2 + (\delta\phi_{b(i)})^2} \quad (33)$$

$$(\delta\phi_{b(i)})^2 = [0\;1]\mathbf{R}(\phi_b)\mathbf{Q}^{-1}_i\mathbf{R}^T(\phi_b)\begin{bmatrix} 0 \\ 1 \end{bmatrix} \quad (34)$$

$$\hat{\rho} = \frac{\sin(\hat{\phi}_b - \phi_{b(i)})}{\Delta l\sin(\hat{\phi}_b + 0.5\,\kappa\,\Delta l)} \quad (35)$$

$$q^{-1}_{\rho(i)} = [q_{\rho(i-1)} + q_{\phi(i)}]^{-1} + n_{\Delta l} \quad (36)$$

where $n_{\Delta l}$ is the process noise caused by uncertainty in the step size. The new estimate, $\tilde{\rho}_i$, should be substituted into (24) for ρ_i. Note that the step size for the Kalman filter does not have to be the same as the step size used in the calculating the steering sequence.

A Kalman filter is required for each active marker. However, only one Kalman filter will receive a bearing measurement at a given instant because the camera pan can only fixate on one marker. Thus, the attention of the camera must be switched from marker to marker to obtain a useful interpretation of the local environment. In this paper it is assumed that some higher-level agent has selected the order in which the markers will be visited. This ordering is the primary criteria for attention: the current marker will receive the most attention. There are instants when additional viewing of the current marker provides only minimal additional information. For example, if the error covariance of the bearing angle, obtained from (34), is small, the integration of new bearing measurements have little effect. In such cases, it is useful to temporarily shift the camera gaze to the next marker.

A criterion is needed to determine when attention can be switched from the current marker, and how far the vehicle can travel before attention must be re-directed to the current marker. The state transition equations, (24) and (26), can predict increases in the future error covariance if no new measurements are made. If a threshold error covariance is selected, say equal to the measurement uncertainty $(\delta\hat{\phi})^2$, the number of steps that can be traveled before reaching this threshold is a good criterion for judging the novelty of future data. If the number of steps is large, the computer can temporarily shift attention to the next marker.

6. Implementation and Results

This section presents three groups of simulations. The first group demonstrates two simple maneuvers with well-behaved initial conditions for the cases of non-zero and zero heading error weights. The second group illustrates the robustness of the algorithm to range errors and to awkward initial conditions. The final group demonstrates the range estimation and attention switching.

The parameters and key equations used in the implementation are listed below. The basic steering algorithm is defined by (15). The control horizon is $N = 10$. The weights for the lateral error, heading error, curvature penalty, change in curvature penalty, and endpoint constraints are selected as $\lambda_b = 1$, $\lambda_h = 60$, $\lambda_\kappa = 60$, $\lambda_{\Delta\kappa} = 6$, and $\lambda_{ref} = 6$, respectively. The dimensional units for each weight are as follows: λ_b is $(\text{dist})^{-2}$ where (dist) is an arbitrary distance measure; λ_h is $(\text{radians})^{-2}$; λ_κ, $\lambda_{\Delta\kappa}$, and λ_{ref} are $(\text{dist/radians})^2$. The most important relationship between the weights is the ratio of λ_h and λ_b. The important nonlinear parameters for the robust steering include the maximum steering angle and the dynamic heading error (see (19)). It is assumed that the maximum steering angle of the vehicle produces a curvature of 0.1 radians/dist. The threshold heading angle, ϕ_T, used by the dynamic heading weight is $\frac{3}{4}\pi$.

An important tool for evaluating the steering algorithm is the phase plane plot comprising bearing angle and heading error. The phase plane plot has interesting properties: it is independent of range; and it has a constant slope for a heading error weight of zero. The slope of the trajectory is

$$\frac{\delta\phi_b}{\delta\phi} = 1 - \frac{\rho}{\kappa_1}\sin\phi_b. \quad (37)$$

From (17) and (18), it can be seen that

$$\frac{\rho}{\kappa_1}\sin\phi_b = N^{-2}[(N-0.5) + (N-1.5)\frac{\kappa_2}{\kappa_1} + \cdots + 0.5\frac{\kappa_N}{\kappa_1}], \quad (38)$$

which is not dependent on the range to the marker. When the weight on the heading error is set to zero, the slope of the trajectory is constant:

$$\frac{\delta\phi_b}{\delta\phi} \approx 1 - N^{-2}\sum_{i=1}^{N}\frac{(N-i+0.5)^2}{(N-0.5)}. \quad (39)$$

For $N = 10$, the slope of the trajectory is 0.65.

Well-behaved Initial Conditions: Figure 2 illustrates a "lane change:" a maneuver whose initial and final headings are equal. Since there is a heading constraint at the marker, the heading error weight is non-zero ($\lambda_h > 0$). Figure 2 contains the top view of the path traveled by the vehicle for specific initial conditions and the bearing angle-heading error phase plane plot for various well-behaved initial conditions. The path traveled is smooth containing one inflection point. All the phase plane trajectories have the same shape, approaching the origin (destination) along a line of slope 0.65. The phase plane trajectories illustrate the value of using the sensory feedback mode. Despite the fact that the heading error is as large as $\frac{3}{4}\pi$ (making the linearization used in (5) invalid), the initial portion of the feedforward path is sufficiently accurate that recalculating κ_1 after each step allows the vehicle to reach the destination.

Figure 3 shows a maneuver with similar initial conditions as the previous example when the heading error weight is set to zero. The path curvature is initially large and shrinks as the range to the destination decreases. All phase plane trajectories terminate at the line $\phi_b = 0$ and have a slope of 0.65 (as predicted by (39)). The phase plane illustrates that the vehicle can be realigned with the destination by reducing the heading error weight to zero, if $|\phi_b| < \frac{\pi}{2}$.

Robustness: Robustness to range errors is illustrated in figure 4, which contains three paths whose range estimates are half, equal, and double the actual range. In each case, the vehicle reaches the destination. However, the underestimated (overestimated) range causes the steering to be more lively (sluggish).

The next example illustrates the robustness to awkward initial conditions provided by introducing non-linearities into the steering algorithm. Figure 5 shows the path traveled by, and the phase plane of, a vehicle that has backtracked and returned to its original heading. The phase plane plot illustrates the effect of the steering non-linearity. The steering non-linearity prevents the vehicle from diverging from the destination, keeping the bearing angle near $-\frac{\pi}{2}$, causing the vehicle to "orbit" the destination. Once the heading error is sufficiently small, the basic steering algorithm directs the vehicle to the destination at the desired heading. Figure 5 also shows a maneuver, with the same destination position and heading as before, using the dynamic heading error weight. The path traveled and the phase plane trajectory are much smoother.

Estimation and Attention Switching: The following examples demonstrate the range estimation to, and attention switching between, markers in the presence of measurement noise. Gaussian noise with a standard deviation of 1.1 degrees (0.02 radians) is added to the measured bearing angle. Figure 6 shows the range error (the difference between the estimated and actual range), along with the estimated standard deviation (derived from q_ρ^{-1} of (36)), for the maneuver shown in figure 2. At long ranges, during the initial part of the maneuver, the estimated range is sensitive to bearing angle uncertainty, as illustrated by the large error covariance. As the vehicle approaches the marker, the error covariance and the range error decrease.

Figure 7 shows the range error for a maneuver passing two

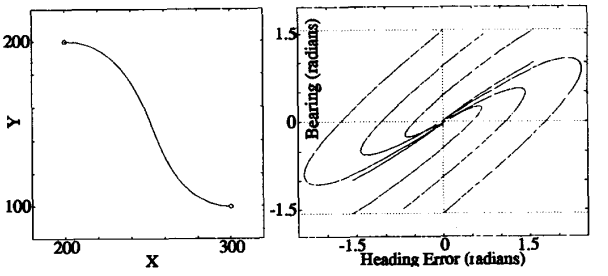

Figure 2: Well-behaved maneuver for non-zero heading error weight. (Left) Path traveled for initial conditions $(\phi_b, \phi_{h,m} - \phi_h) = (\frac{\pi}{4}, 0)$ and $(x_0, y_0) = (200, 200)$. (Right) Bearing angle-heading error phase plane plot for various well-behaved initial conditions. All phase plane trajectories terminate at the origin.

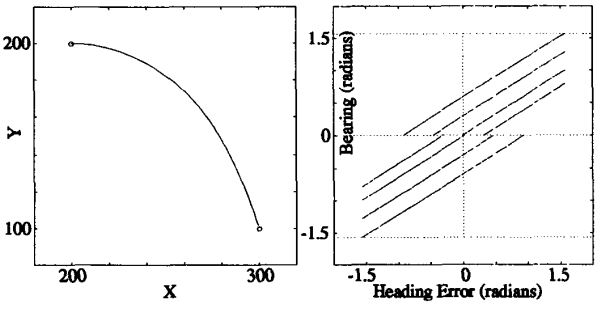

Figure 3: Well-behaved maneuver for zero heading error weight. (Left) Top view of path traveled for initial conditions $(\phi_b, \phi_{h,m} - \phi_h) = (\frac{\pi}{4}, 0)$ and $(x_0, y_0) = (200, 200)$. (Right) Phase plane plot for various well-behaved initial conditions. All phase plane trajectories terminate at the line $\phi_b = 0$ and have a slope of 0.65.

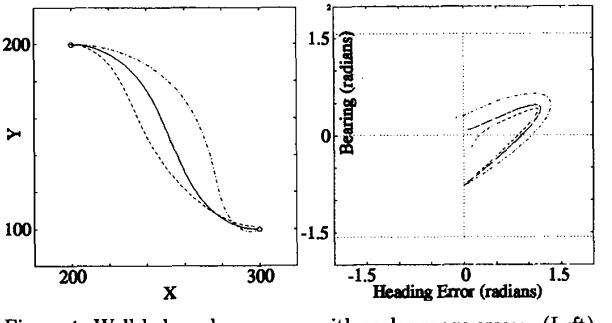

Figure 4: Well-behaved maneuver with scalar range errors. (Left) Paths traveled based on estimated ranges that are half (dashed), equal (solid), and double (dot-dash) the actual range. (Right) Phase plane plots. Note that the underestimated (overestimated) range causes the steering to be more lively (sluggish).

markers. The initial position of the vehicle is $(x_0, y_0) = (200, 200)$. The positions of marker 1 and marker 2 are (300, 100) and (400, 200), respectively. The desired heading at each marker is equal to the initial vehicle heading. The maneuver to marker 1 is the same as figure 2; the maneuver from marker 1 to marker 2 has a similar, but reversed, shape. The attention of the camera is focused on marker 1 during the path intervals $l = 0$ to 56 and $l = 98$ to 148, and on marker 2 during the intervals $l = 58$ to 96 and $l = 150$ to 300. The previewing of marker 2 during the interval $l = 58$ to 96 is performed when the bearing angle to marker 1 is near zero (the range information provided by movement along a zero bearing angle is minimal, as can be seen by (33)). Previewing marker 2 greatly reduces the error in later range estimates ($l = 170$ to 300). The improvement is due to the fact that the measurements made during interval $l = 58$ to 96 view marker 2 from a much different direction than measurements made during the interval $l = 150$ to 300. Thus, the bearing angle error covariance matrix Q^{-1} is reduced, and the range accuracy is improved.

7. Conclusion

This paper has presented an algorithm for steering a moving vehicle to a visible marker. The algorithm, whose primary measurement is the marker bearing, is robust to range errors and to awkward initial conditions. The primary contributions of this paper are (a) the dynamic heading error weight and the steering nonlinearity used to ensure robustness to awkward initial conditions, and (b) the criteria for switching camera attention for multiple markers.

References

[1] R. G. Brown, *Introduction to Random Signal Analysis and Kalman Filtering.* New York, NY: Wiley and Sons, 1983.

[2] D. W. Clarke, C. Mohtadi, and P. S. Tuffs, "Generalized predictive control—part I. The basic algorithm," *Automatica,* vol. 23, no. 2, pp. 137-148, 1987.

[3] E. D. Dickmanns and B. D. Mysliwetz, "Recursive 3-D road and relative ego-state recognition," *Trans. Pattern Anal. Machine Intell.*, vol. 14, no. 2, pp. 199-213, 1992.

[4] A. Elfes, "Using occupancy grids for mobile robot perception and navigation," IEEE Computer, pp. 46-57, 1989.

[5] D. Feng and B. H. Krogh, "Dynamic steering control of conventionally steered mobile robots," *Journal of Robotic Systems,* vol. 8, no. 5, pp. 699-721, 1991.

[6] Y. Kanayama and B. I. Hartman, "Smooth local path planning for autonomous vehicles," in *Proc. Int. Conf. Robotics and Automation*, Scottsdale, AZ, 1989, pp. 1265-1270.

[7] W. L. Nelson, "Continuous steering-function control of robot carts," *IEEE Trans. on Industrial Electronics,* vol. 36, no. 3, pp. 330-337, 1989.

[8] D. H. Shin and S. Singh, "Vehicle and path models for autonomous navigation," C. E. Thorpe (ed.), *Vision and Navigation—the Carnegie Mellon Navlab.* Kluwer, 1990.

[9] T. L. Song and J. L. Speyer, "A stochastic analysis of a modified gain extended Kalman filter with applications to estimation with bearing only measurements," *IEEE Trans. on Automatic Control,*, vol. 30, no. 10, pp. 940-949, 1985.

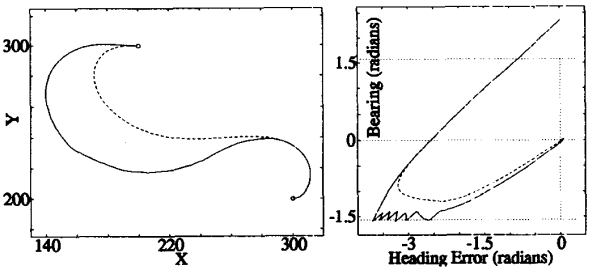

Figure 5: Maneuver with awkward initial conditions, $|\phi_b| > \frac{\pi}{2}$, with fixed (solid) and dynamic (dashed) heading error weights. (Left) Top view of the path originating from $(x_0, y_0) = (300, 200)$. (Right) Phase plane plot. The phase plane trajectory for the fixed heading error weight, λ_h, is not smooth due to the repeated application of the steering nonlinearity.

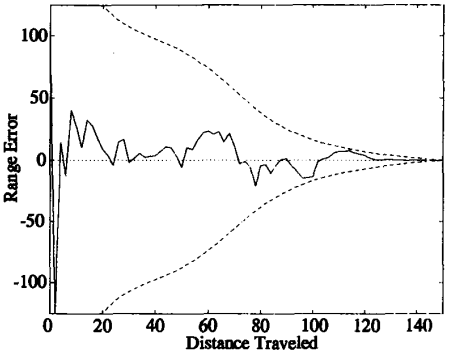

Figure 6: Range error (solid) and estimated standard deviation (dashed) for maneuver in figure 1 when the measured bearing angle is corrupted by noise $|\delta\hat{\phi}_b| = 1.1$ degrees.

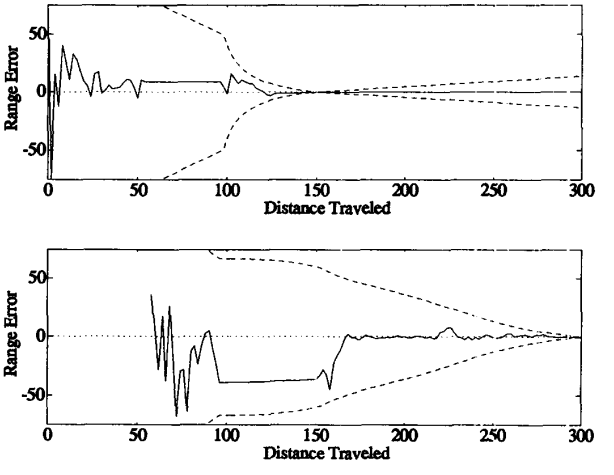

Figure 7: Range error (solid) and estimated standard deviation (dashed) for a two marker maneuver with attention switching. (Top) Marker 1. (Bottom) Marker 2. Marker 1 is passed at a distance $l = 150$, marker 2 is reached at $l = 300$. Attention is fixed on marker 1 during the intervals $l = 0$ to 56 and $l = 98$ to 148, and on marker 2 during the intervals $l = 58$ to 96 and $l = 150$ to 300.